








Recombination and spin dynamics of excitons in thin (Ga,Al)(Sb,As)/AlAs quantum wells with an indirect band gap and type-I band alignment

T. S. Shamirzaev ^{1,3} D. R. Yakovlev ^{2,4} A. K. Bakarov ¹ N. E. Kopteva ² D. Kudlacik ²
A. K. Gutakovskii ¹ and M. Bayer ^{2,4}

¹*Rzhanov Institute of Semiconductor Physics, Siberian Branch of the Russian Academy of Sciences, 630090 Novosibirsk, Russia*

²*Experimentelle Physik 2, Technische Universität Dortmund, 44227 Dortmund, Germany*

³*Ural Federal University, 620002 Yekaterinburg, Russia*

⁴*Ioffe Institute, Russian Academy of Sciences, 194021 St. Petersburg, Russia*



(Received 1 August 2020; revised 8 September 2020; accepted 12 October 2020; published 27 October 2020)

The dynamics of exciton recombination and spin relaxation in thin (Ga,Al)(Sb,As)/AlAs quantum wells (QWs) with indirect band gap are studied. The band alignment in these QWs is identified as type I. The exciton recombination time exceeds hundreds of microseconds, while the spin relaxation times of the electron and the heavy hole in an exciton do not exceed hundreds of nanoseconds. The heavy-hole longitudinal g factor is determined to be $+2.5$. Despite the long exciton lifetimes, the photoluminescence circular polarization degree induced by a magnetic field is unexpectedly small and does not exceed 25%.

DOI: [10.1103/PhysRevB.102.165423](https://doi.org/10.1103/PhysRevB.102.165423)

I. INTRODUCTION

The prospects for constructing quantum information devices have initiated numerous fundamental and applied studies of the charge carrier spin dynamics in solid state systems [1–3]. A common approach to study spin dynamics is creating an imbalance in the spin system through a nonequilibrium population of spin states. In direct band gap semiconductor heterostructures with a large oscillator strength of the radiative transitions, a nonequilibrium spin population can be created by optical orientation of excitons with circularly polarized light [4]. In this case, the light delivers angular momentum to the electron system, inducing its spin polarization, which subsequently decays due to spin relaxation processes. The spin dynamics can be measured by the decay of the photoluminescence (PL) circular polarization degree [4]. A convenient alternative to optical orientation is study of the electron spin dynamics, e.g., in structures with weak exciton-photon interaction, in a longitudinal magnetic field inducing a Zeeman splitting of the exciton states [5]. Here one can use nonresonant, unpolarized, or linearly polarized light for PL excitation, which does not introduce angular momentum into the electronic system. Therefore, right after the moment of excitation no spin polarization is present, since the magnetic-field-split exciton states will be populated equally. As time passes by, spin relaxation processes tend to bring the populations of exciton states toward the values expected from an equilibrium (Boltzmann) distribution. As a result, a net exciton spin polarization emerges, which can be measured in the dynamics of the PL circular polarization degree as an increase of its polarization degree starting from zero [5–7].

In well-studied direct band gap semiconductor quantum wells (QWs) and quantum dots (QDs), such as those based on the material combinations (In,Ga)As/GaAs or GaAs/(Al,Ga)As, the typical exciton recombination times are

in the range of several nanoseconds [8], which is noticeably shorter than the exciton spin relaxation times [9]. Indeed, as was shown in numerous theoretical studies [10,11], carrier localization suppresses the mechanisms that determine the spin relaxation of freely moving electronic excitations, such as the Elliot-Yafet and Dyakonov-Perel mechanisms. As a result, the spin relaxation time of localized excitons can reach milliseconds, as confirmed experimentally [12]. Therefore, for studying the localized exciton spin dynamics experimentally, heterostructures with long exciton lifetimes, which are comparable to their spin relaxation times, are required. Recently, we demonstrated that tailored III-V semiconductor QWs and QDs with an indirect band gap can serve as model systems for studying spin dynamics in this situation. In these structures, the momentum conservation law prohibits the exciton recombination and, thus, the exciton lifetimes extend up to hundreds of microseconds or even milliseconds [5,13–20]. One promising system among these structures is the combination of GaSb and AlAs into heterostructures. Our calculations and experimental data show that (Ga,Al)Sb/AlAs QWs can be fabricated with type-I or type-II band alignment, but both with indirect band gap resulting in very long exciton lifetimes [20]. However, the magnetic-field-induced spin polarization and the related spin dynamics of excitons in such QWs have been scarcely studied so far.

In this paper, we investigate the recombination and spin relaxation dynamics of excitons in thin (Ga,Al)(Sb,As)/AlAs QWs with an indirect band gap and a type-I band alignment. We show that in spite of the long (up to hundreds of microseconds) exciton lifetimes, which markedly exceed the spin relaxation times of electrons and holes (hundreds of nanoseconds), the PL circular polarization degree induced by a longitudinal magnetic field varies greatly from sample to sample and is unexpectedly very low, not exceeding 25%.

The paper is organized as follows. In Sec. II the studied heterostructures and used experimental techniques are described. In Sec. III we present the experimental data on the dynamics obtained in external magnetic fields by time-integrated and time-resolved PL. We discuss the data in relation to the theoretical model describing the exciton dynamics developed in Ref. [16]. The conclusions are given in Sec. IV.

II. EXPERIMENTAL DETAILS

The (Ga,Al)(Sb,As)/AlAs QWs studied here were grown by molecular-beam epitaxy on semi-insulating, (001)-oriented GaAs substrates in a Riber Compact system. The structures consist of a layer with a nominal thickness of 0.25 (S1 structure) or 1.0 (S2 and S3 structures) [21] monolayers (ML) of GaSb embedded between 50-nm-thick layers of AlAs, grown on top of a 200-nm-thick GaAs buffer layer. The lower AlAs layer in all structures was grown at the temperature of 620 °C. Then the growth was interrupted, and the substrate temperature was decreased down to 480 °C (for structures S1 and S2) and 500 °C (for structure S3) under As flux during cooling. The AlAs surface had a $c(4 \times 4)$ reconstruction (measured by the reflection high-energy electron diffraction technique). The GaSb layers were deposited at a rate of 0.1 ML/s as calibrated in the center of the wafer, using reference samples. The accuracy of the material deposition was better than 0.05 ML. The upper AlAs layer was grown at the same substrate temperature as the corresponding GaSb layer. A 20-nm-thick GaAs cap layer protects the top AlAs layer against oxidation. The atomic structure was studied by transmission electron microscopy (TEM) using a JEM-4000EX system operated at an acceleration voltage of 200 keV.

For optical experiments the samples were placed in a split-coil magnet cryostat for generating magnetic fields up to $B = 8$ T. The samples were held in pumped liquid helium at temperatures $T = 1.6$ – 1.8 K. The angle θ between the magnetic field direction and the QW growth axis (z axis) was varied between 0° (Faraday geometry) and 45° . Photoluminescence was excited by the third harmonic of a Q -switched Nd:YVO₄ laser (3.49 eV) with a pulse duration of 5 ns. The pulse energy density was kept below 100 nJ/cm² and the pulse-repetition frequency was varied from 300 Hz up to 100 kHz [22]. For time-integrated measurements the excitation power density, P_{ex} , was varied in the range from 0.01 up to 5 W/cm². The emitted light was dispersed by a 0.5-m monochromator. For time-integrated and time-resolved measurements the photoluminescence was detected by a gated charge-coupled-device (CCD) camera, synchronized with the laser via an external trigger signal. The PL dynamics in magnetic field was detected by a GaAs photomultiplier operated in the time-correlated photon-counting mode. When monitoring the PL decay across a wide temporal range up to 2.5 ms, the time resolution of the detection system varied between 10 and 2000 ns.

The exciton spin dynamics were measured using the PL circular polarization degree, P_c , induced by the external magnetic field. It was evaluated from the PL data by $P_c = (I_{\sigma^+} - I_{\sigma^-}) / (I_{\sigma^+} + I_{\sigma^-})$, where I_{σ^+} and I_{σ^-} are the intensities of the σ^+ and σ^- polarized PL components, respectively. To determine the sign of P_c , we performed a control measure-

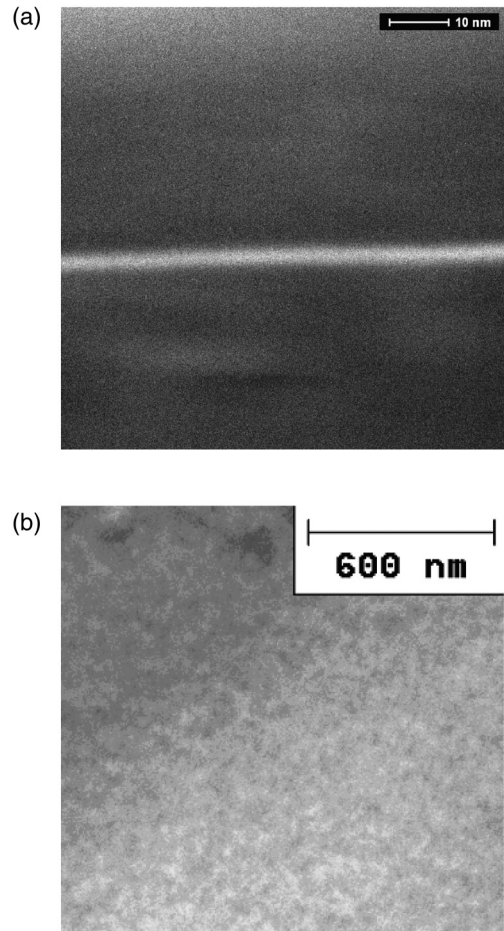


FIG. 1. TEM images for the (Ga,Al)(Sb,As)/AlAs heterostructure S3: (a) cross section, and (b) plane view.

ment on a diluted magnetic semiconductor structure with (Zn,Mn)Se/(Zn,Be)Se quantum wells for which $P_c > 0$ in Faraday geometry [23].

III. EXPERIMENTAL RESULTS

A. Transmission electron microscopy

A cross-section TEM image of the S3 structure is shown in Fig. 1(a). The QW thickness equals 3 nm which strongly exceeds the one monolayer targeted in growth for this structure. Therefore, we conclude that material intermixing occurs so that the QW consists of the quaternary alloy (Ga,Al)(Sb,As). The intermixing is confirmed by measuring the distribution of chemical elements in the 1-ML-thick GaSb/AlAs QW (structure S2) given in our recent paper [24].

It is well known that the driving force of the transition from a two-dimensional to a three-dimensional growth mode (2D-3D transition) in heteroepitaxial systems is the relaxation of the elastic energy of a strained layer due to QD nucleation [25]. The elastic energy depends on the lattice mismatch between the deposited material and the substrate as well as on the thickness of the pseudomorphic deposited layer. There is a critical thickness of this pseudomorphic layer, h_c , corresponding to the critical level of the elastic energy at a given

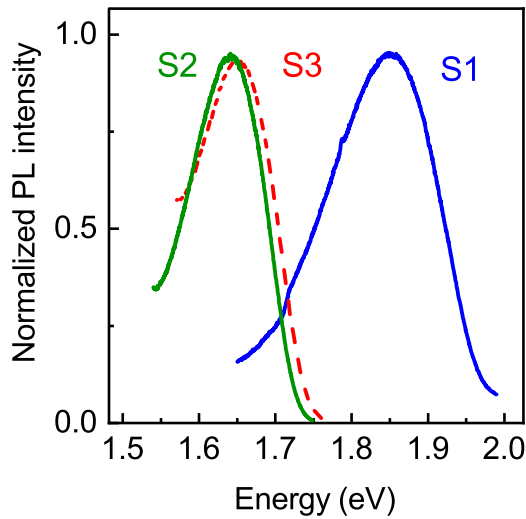


FIG. 2. Normalized time-integrated photoluminescence spectra of the (Ga,Al)Sb/AlAs QWs (samples S1, S2, and S3). The pulse repetition rate of the excitation laser is 100 kHz. $T = 1.8$ K.

lattice mismatch [26,27]. If the thickness of the deposited layer exceeds h_c , QD nucleation is initiated.

Despite the significant mismatch between the AlAs and GaSb lattice constants of 7.1% [28], QDs do not form in the heterostructure due to the decrease of the elastic energy when the materials are mixed [see the plane-view image in Fig. 1(b)]. Since the degree of mixing increases with structure growth temperature [29,30], we conclude that all heterostructures are QWs formed by a (Ga,Al)(Sb,As) alloy sandwiched between AlAs barriers.

B. Photoluminescence

Time-integrated photoluminescence spectra of the studied (Ga,Al)(Sb,As)/AlAs QWs, measured at the temperature of 1.8 K and the pulse repetition rate of 100 kHz, are shown in Fig. 2. The spectra show broad emission bands with maxima (full widths at half maximum) of $E_{\max} = 1.850$ eV (170 meV), 1.640 eV (110 meV), and 1.654 eV (110 meV) for the structures S1, S2, and S3, respectively. The increase of the epitaxy growth temperature from 480 to 500 °C for the fixed nominal GaSb layer thickness of 1 ML leads to a small high-energy shift of the PL band by 14 meV without changing the linewidth; compare in Fig. 2 the spectra for the samples S2 and S3. A decrease of the nominal thickness of the GaSb layer from 1 down to 0.25 ML at fixed growth temperature (samples S2 and S1) is accompanied by a shift of the PL band by 210 meV to higher energy. The dependencies of the spectral position and width of the PL bands on the nominal thickness and growth temperature are similar to the dependencies observed for InSb/AlAs based QWs [31]. As indicated already, they are provided by the intermixing of materials during growth. The large linewidth of the PL spectra of the studied QWs is the result of inhomogeneous broadening of the electron and hole energy levels due to fluctuations of the QW width and composition. The fluctuations are caused by the spatially inhomogeneous antimony segregation when overgrowing a thin GaSb layer with aluminum

arsenide [24]. Thus, the QWs are formed by relatively thick layers of (Ga,Al)(Sb,As) alloy with strong spatial fluctuations of the composition both in the QW plane and along the growth direction.

We demonstrated recently that QWs and QDs formed in the GaSb/AlAs heterosystem can have type-I or type-II band alignments [13,20]. A method for identifying the type of band alignment in QWs with heterointerface fluctuations was proposed recently [24]. It was shown that in such structures the PL maximum, E_{\max} , measured as a function of the excitation power density, P_{ex} , is generally described by the following expression:

$$E_{\max}(P_{\text{ex}}) - E_{\max}(P_0) = (U_e + U_h) \ln(P_{\text{ex}}/P_0) + b(P_{\text{ex}}/P_0)^{1/3}. \quad (1)$$

Here U_e and U_h are the parameters of the Urbach energy tails for electrons and holes, respectively, P_0 is the minimum value of the used excitation power density, and b is a variable parameter. The logarithmic term describes the effect of electronic state filling for QWs of both type I and type II. The second term takes into account the band bending, which appears with increasing charge carrier concentration in the type-II QWs due to spatial separation of the carriers but it is absent in type-I QWs where $b \equiv 0$.

We also showed recently already that the (Ga,Al)(Sb,As)/AlAs QWs with 1-ML nominal thickness (heterostructures S2 and S3) have a type-I band alignment [24]. To determine the type of band alignment for the S1 heterostructure, we measured the PL line position as a function of excitation power density in the range of a linear increase of the integrated PL intensity [24]. The shape of the spectra remains practically unchanged with an increase in excitation power within the full range of used P_{ex} as shown in the bottom inset of Fig. 3. The dependence of the PL line shift on the excitation power density [$E_{\max}(P_{\text{ex}}) - E_{\max}(P_0)$ for $P_0 = 1.7 \times 10^{-2}$ W/cm²] shown in Fig. 3 is well described by the logarithmic term in Eq. (1). Therefore, we conclude that the S1 structure has a band alignment of type I, similar to the structures S2 and S3.

The dynamics of the unpolarized PL intensity measured at the PL maximum of the S1 and S2 structures are shown in Fig. 4. The recombination dynamics shows two distinct stages: (i) a fast nonexponential decay during the first microsecond after the excitation pulse, which is followed by (ii) an exponential decay with times of $\tau_R^{S1} = 0.29$ ms and $\tau_R^{S2} = 0.32$ ms for the S1 and S2 samples, respectively. Since more than 95% of the PL intensity in the time-integrated spectra is collected in the time range exceeding one microsecond, we focus in our analysis on the long-term dynamics.

In a longitudinal magnetic field of 8 T, the decay time of the long-term component increases in both structures; see Fig. 5. In the S2 structure it grows by a factor of four (from 0.32 up to 1.22 ms), while in the S1 structure it increases by 45% only (from 0.29 up to 0.42 ms). As we showed lately, the increase of the exciton recombination time is a result of the relaxation from the bright to the dark exciton state when the exciton Zeeman splitting exceeds the thermal energy $k_B T$ [15,16]. Here k_B is the Boltzmann constant.

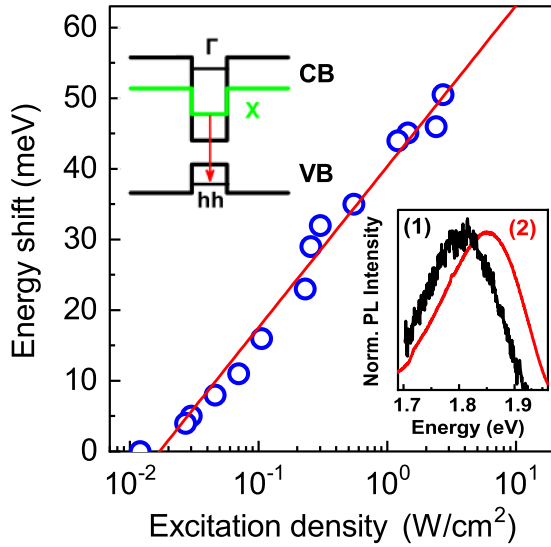


FIG. 3. Energy shift of the PL band maximum in the S1 structure as a function of excitation density. The solid line gives the dependence according to $E_{\max}(P_{\text{ex}}) - E_{\max}(P_0) = 9.9 \times \ln(P_{\text{ex}}/P_0)$ meV with $P_0 = 1.7 \times 10^{-2} \text{ cm}^{-2}$. The upper inset shows schematically the band structure. The Γ and X valleys of the conduction band are presented in black and green colors, respectively. The red arrow marks the optical transition of the ground state exciton responsible for the photoluminescence. The bottom inset shows the normalized PL spectra of the QW measured at excitation densities equal to (1) 0.05 and (2) 4 W/cm^2 .

C. Magnetic-field-induced circular polarization of photoluminescence

In order to obtain the parameters of the exciton fine structure, we measured time-integrated PL spectra in σ^+ and σ^- polarization in a longitudinal magnetic field up to 8 T.

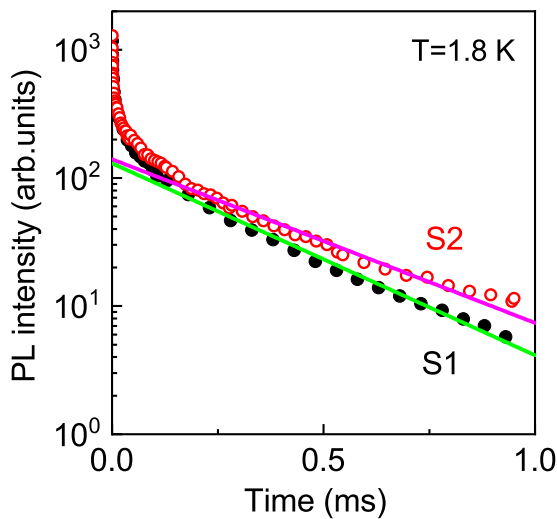


FIG. 4. PL dynamics at the emission maximum of the S1 (1.85 eV) and S2 (1.65 eV) QWs. The pulse repetition rate is 1 kHz. The laser pulse ends at 10 ns. $T = 1.8 \text{ K}$, $B = 0 \text{ T}$. The solid lines give monoexponential fits of the decay with $\tau_R^{S1} = 0.29 \text{ ms}$ (green) and $\tau_R^{S2} = 0.32 \text{ ms}$ (magenta).

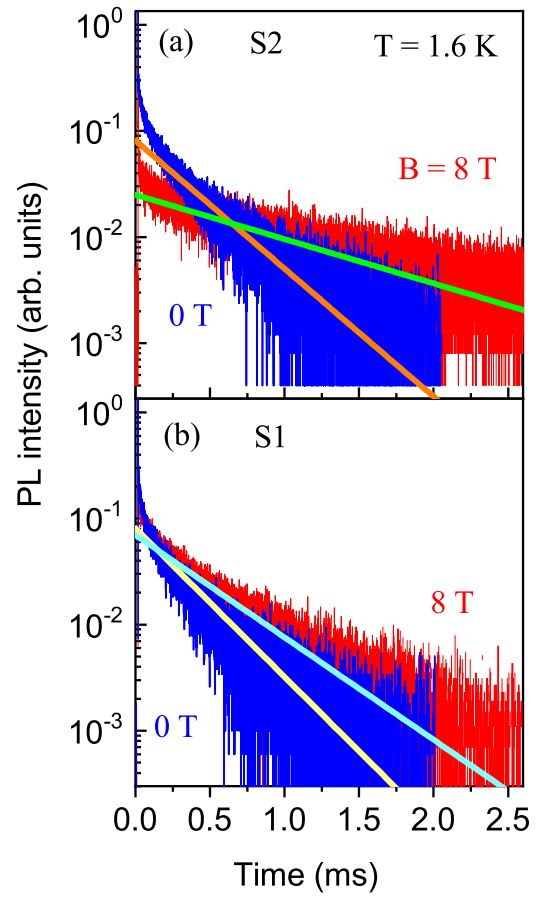


FIG. 5. Recombination dynamics measured at the PL maximum in longitudinal magnetic fields of $B = 0$ and 8 T. (a) S2 sample dynamics recorded at 1.65 eV. The solid lines are monoexponential fits with $\tau_R^{S2}(0 \text{ T}) = 0.32 \text{ ms}$ (orange) and $\tau_R^{S2}(8 \text{ T}) = 1.22 \text{ ms}$ (green). (b) S1 sample dynamics recorded at 1.85 eV. The lines are fits with $\tau_R^{S1}(0 \text{ T}) = 0.29 \text{ ms}$ (yellow) and $\tau_R^{S1}(8 \text{ T}) = 0.42 \text{ ms}$ (cyan). The pulse repetition rate is 300 Hz. The laser pulse ends at 10 ns. $T = 1.6 \text{ K}$.

Surprisingly, we do not observe any circular polarization of the PL for the S1 structure with the nominal thickness of 0.25 ML. Therefore, we focused on the 1-ML structures S2 and S3. Circular polarization-resolved PL spectra of the S2 structure measured at $B = 6 \text{ T}$ are shown in Fig. 6. The σ^- -polarized PL component is more intense than the σ^+ -polarized one, so that P_c is negative. The polarization degree at the maximum of the PL band equals -0.1 . The S3 structure shows the same polarization degree at $B = 6 \text{ T}$. Therefore, we present and discuss below the typical behavior measured for the S2 structure.

The magnetic field dependencies of P_c measured at the PL maximum in Faraday geometry ($\theta = 0^\circ$) and for tilted field ($\theta = 45^\circ$) are shown in Fig. 7(a). The $P_c(B)$ behavior is unusual as it behaves nonmonotonically in Faraday geometry. Its value increases from zero up to -0.07 with increasing field strength up to 4 T, but decreases in stronger fields. In tilted-field geometry ($\theta = 45^\circ$), $P_c(B)$ monotonically increases, reaching -0.19 at $B = 8 \text{ T}$.

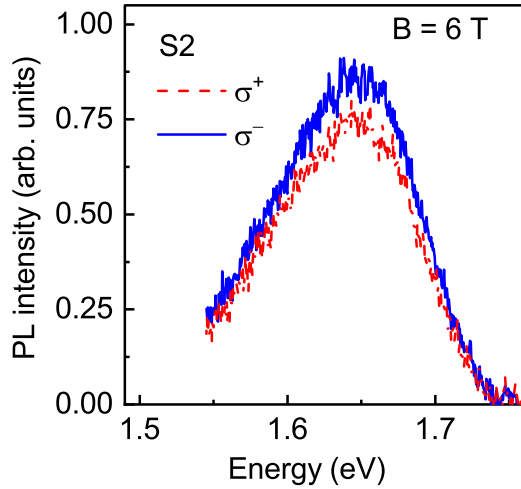


FIG. 6. Time-integrated PL spectra measured in Faraday geometry ($B \parallel z$) in σ^+ and σ^- polarization. $T = 1.8$ K. The pulse repetition rate is 800 Hz and the emission is integrated over the temporal range of 0–1.25 ms.

The time evolution of P_c after pulsed excitation measured at $B = 8$ T in the S2 structure is shown in Fig. 7(b). It is unusually nonmonotonic. During the initial rising stage extended over the first 400 ns, P_c reaches -0.24 and then it decreases down to -0.05 for time delays up to 1 ms.

In (Ga,Al)(As,Sb)/AlAs QW structures with type-I band alignment the indirect exciton is formed by a Γ -point heavy hole with angular momentum $j = 3/2$ and an electron with $s = 1/2$ spin in the X valley of the conduction band. Both carriers are localized within the (Ga,Al)(As,Sb) layer. The corresponding band diagram for the indirect band gap structures with a type-I band alignment is shown in the inset of Fig. 3. Accounting for the angular momentum of electron and hole results in four exciton fine structure states. The two bright exciton states are characterized by the angular momentum projections ± 1 onto the growth axis z and the two dark states by the projections ± 2 [15,16]. In spite of the restrictions imposed by the momentum conservation law, the spin selection rules allow phonon-assisted radiative recombination of bright excitons. The dark excitons are optically inactive (radiative recombination is forbidden by spin selection rules); they recombine with a nonradiative decay rate, and thus have a longer lifetime so that they can act as a reservoir of excitons. In magnetic field the excitons undergo the Zeeman splitting, as shown schematically in Fig. 8. The hole eigenstates are still characterized by the z component of the angular momentum, $j_z = \pm 3/2$, and denoted in short by the state vectors $|\pm 3/2\rangle_z$. The electron eigenstates $|s\rangle_B$ are characterized by the spin component projection $s = \pm 1/2$ onto the magnetic field direction. The exciton spin state is given by the product of the electron and heavy-hole eigenstates

$$|sj_z\rangle = |s\rangle_B |j_z\rangle_z.$$

The occupancies, f_{sj_z} , of the exciton Zeeman sublevels are controlled by the interplay between recombination processes and spin flips of either electron or hole between the sublevels. They can be described by a set of kinetic equations given in

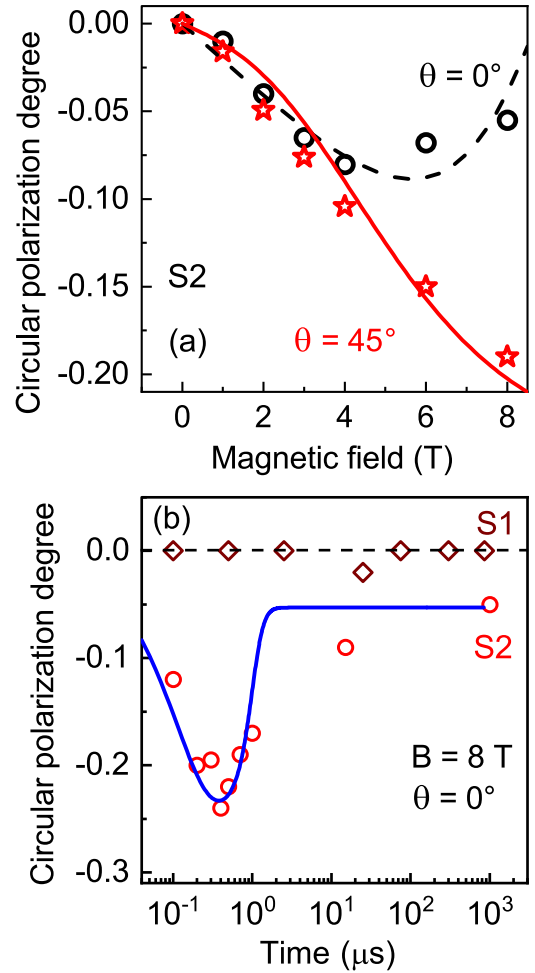


FIG. 7. (a) Magnetic field dependence of the polarization degree measured at the maximum of time-integrated PL for structure S2 in the Faraday ($\theta = 0^\circ$) and tilted-field ($\theta = 45^\circ$) geometries. $T = 1.8$ K. The solid and dashed lines show the model results with parameters given in the text. (b) Dynamics of P_c at the PL maximum for the S1 and S2 structures measured in the Faraday geometry at $B = 8$ T. $T = 1.8$ K. The pulse repetition rate is 800 Hz; the laser pulse ends at 10 ns. The solid line shows the model results with parameters given in the text. The dashed line at $P_c = 0$ is a guide to the eye.

Ref. [16]:

$$\begin{aligned} \frac{df_{sj_z}}{dt} + (W_{\bar{s},s} + W_{\bar{j}_z,j_z}^z) f_{sj_z} - W_{s,\bar{s}} \bar{f}_{\bar{s}j_z} - W_{j_z,\bar{j}_z} f_{s\bar{j}_z} + \mathcal{R} f_{sj_z} \\ = G_{sj_z}. \end{aligned} \quad (2)$$

Here $\bar{s} = -s$, $\bar{j}_z = -j_z$, $W_{s,s'}$ (W_{j_z,j_z}^z) are the electron (heavy-hole) spin-flip rates for the transitions $s' \rightarrow s$ ($j_z' \rightarrow j_z$), the operator \mathcal{R} describes the radiative and nonradiative recombination of excitons, and G_{sj_z} is the exciton generation rate in the state $|sj_z\rangle$ [16].

The rates of the spin-flip transitions from the lower to higher and from the higher to lower Zeeman sublevels are

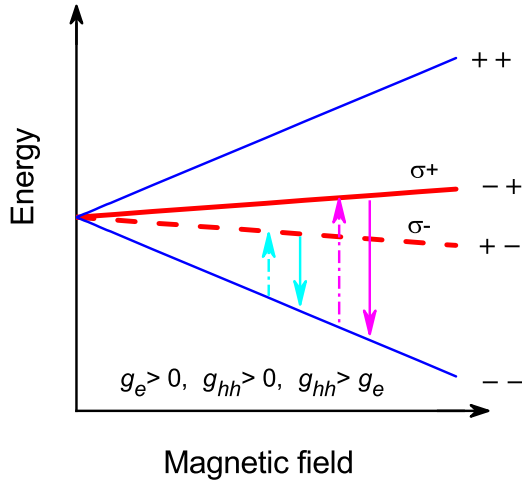


FIG. 8. Scheme of the exciton spin structure in magnetic field, applied in the Faraday geometry $B \parallel z$. The blue lines show the optically dark (spin-forbidden) states. The red lines show the bright (spin-allowed) states that result in σ^+ (solid line) and σ^- (dashed line) polarized emission. The arrows indicate electron (hole) spin-flip processes increasing (dash-dotted) and decreasing (solid) the energy, respectively. For definiteness, the case of positive g_e and g_{hh} with $g_{hh} > g_e$, which provides an explanation of the main experimental findings, is shown.

different and can be interrelated as

$$W_{1/2,-1/2} = W_{-1/2,1/2} \exp\left(-\frac{g_e \mu_B B}{k_B T}\right),$$

$$W_{3/2,-3/2} = W_{-3/2,3/2} \exp\left(-\frac{g_{hh} \mu_B B}{k_B T}\right). \quad (3)$$

Here μ_B is the Bohr magneton, g_e and g_{hh} are the electron and heavy-hole Landé factors, B is the total magnetic field, B_z is its z component. In the experiment the Zeeman splittings can become comparable with the thermal energy, $k_B T$. In accordance with the notation of Ref. [16], $W_{-1/2,1/2} \equiv w_e$ and $W_{-3/2,3/2} \equiv w_h$.

In the framework of the model developed in Ref. [16], the exciton photoluminescence intensity and polarization are governed by the following set of parameters: (i) the values and signs of the electron and hole g factors (in combination with the strength and orientation of the magnetic field), (ii) the radiative (τ_r) and nonradiative (τ_{nr}) recombination times, the spin relaxation rates ($w_e = \tau_{se}^{-1}$, $w_h = \tau_{sh}^{-1}$, where τ_{se} and τ_{sh} are the spin relaxation times for electrons and heavy holes, respectively), describing the spin-flip rates for downward transitions, i.e., from the upper to the lower Zeeman sublevel, and (iii) the temperature, which determines the ratio of the upward and downward transitions.

A deviation of the optical selection rules can be described in the following manner [16]:

$$P_c = \xi \frac{f_{+1} - f_{-1} + C_d(f_{-2} - f_{+2})}{f_{+1} + f_{-1} + C'_d(f_{-2} + f_{+2})}, \quad (4)$$

where $f_{\pm 1}$ and $f_{\pm 2}$ are the occupancies of the bright and dark exciton states, respectively, ξ is a depolarization factor, and the positive coefficients $C_d, C'_d \ll 1$ account for the emission of the dark states. Setting $\xi = 1$ and $C_d, C'_d = 0$,

TABLE I. Parameters for the studied (Ga,Al)(Sb,As)/AlAs QW evaluated from best fits to the experimental data. The parameters for a similar GaAs/AlAs QW, taken from Ref. [16], are given for comparison.

Parameter	Value		Comment
	(Ga,Al)(Sb,As)/AlAs	GaAs/AlAs [16]	
g_e	+2.0	+2.0	[32,33]
$g_{hh\parallel}$	$+2.5 \pm 0.1$	$+3.5 \pm 0.1$	
τ_r	0.32 ms	0.34 ms	
τ_{nr}	2.1 ± 0.2 ms	8.5 ms	
τ_{sh}	30 ± 2 ns	3 ± 0.5 μ s	
τ_{se}	100 ± 5 ns	33 ± 1 μ s	
ξ	0.25	0.75	
C_d	0.002	0.001	
P_c	-0.06	-0.6	$B = 6$ T

we come back to the strict selection rules. In the following, for simplicity, we set $C_d = C'_d$. The details of the model to describe the recombination and spin dynamics of the excitons are presented in Ref. [16].

We demonstrated recently that although the dynamics of the exciton fine structure level populations are determined by a large number of parameters, all of them can be unambiguously determined by describing several experimental dependencies of the PL circular polarization degree in longitudinal and tilted magnetic fields with a unified set of parameters [15–17]. Proceeding in that way with the dependencies presented in Figs. 7(a) and 7(b) allows us to evaluate the longitudinal g factor of the heavy hole, the spin relaxation times of the electron and the heavy hole, as well as the factor describing the radiative recombination of optically inactive excitons, and the PL depolarization parameter. The parameters obtained from best fits are collected in Table I.

It is interesting to compare the parameters obtained for the thin (Ga,Al)(Sb,As)/AlAs QW with that for a similar thin GaAs/AlAs QW [16]; see Table I. One can see that (1) the values of the electron and the heavy-hole longitudinal g factors and (2) the factor describing the radiative recombination of dark excitons in these two systems are close to each other, as one may expect. However, surprisingly, in spite the conditions $\tau_r \gg \tau_{se}, \tau_{sh}$ being fulfilled for both systems, the carrier spin relaxation times τ_{se} and τ_{sh} in the (Ga,Al)(Sb,As)/AlAs QW are several orders of magnitude shorter than the corresponding times in the GaAs/AlAs QW. We demonstrated recently that the spin relaxation in longitudinal magnetic field is mediated by the spin-orbit interaction through phonon scattering [7]. Therefore, a possible reason for the short spin lifetime can be the stronger spin-orbit interaction in the antimonium-based Ga(Sb,As)/AlAs QW, as shown in Ref. [34].

In addition, the PL in the monolayer-thick GaAs/AlAs QW shows a high degree of circular polarization induced by the magnetic field (the PL depolarization parameter ξ equals 0.75, which corresponds to $P_c = -0.6$ at $B = 6$ T), while the PL in the monolayer-thick (Ga,Al)(Sb,As)/AlAs QW is strongly depolarized $\xi = 0.25$ (corresponding to $P_c = -0.06$ at $B = 6$ T). An even more unexpected result is the absence

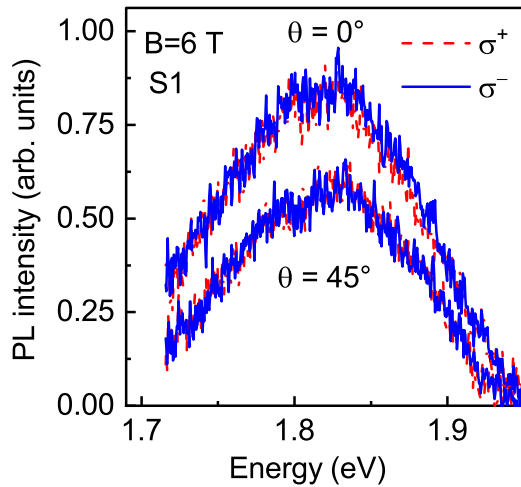


FIG. 9. Time-integrated PL spectra of the S1 structure in longitudinal $\theta = 0^\circ$ (upper curves) and tilted $\theta = 45^\circ$ (bottom curves) magnetic fields of 6 T, recorded for σ^+ and σ^- polarization. $T = 1.8$ K. The pulse repetition rate is 800 Hz. The emission is integrated over the temporal range of 0–1.25 ms.

of circular polarization in a longitudinal magnetic field for the S1 QW with a nominal GaSb layer thickness of 0.25 ML.

In principle, a P_c that is basically identical to zero in time-integrated PL can be realized in several specific ways. The first way corresponds to a situation with identical values of the electron and heavy-hole longitudinal g factors, $g_e = g_{hh\parallel}$, which results in a small exciton Zeeman splitting. This assumption can be easily verified experimentally. Since the electron g factor is isotropic, while the heavy-hole g factor is strongly anisotropic [32], we can break the equality of these g factors in tilted magnetic fields. The PL spectra of the S1 structure in a longitudinal $\theta = 0^\circ$ and tilted $\theta = 45^\circ$ magnetic field of 6 T, measured in σ^+ and σ^- polarization, are shown in Fig. 9. One can see that the PL remains unpolarized even in tilted magnetic field. Therefore, we conclude that the equality of the electron and heavy-hole longitudinal g factors does not play a decisive role for the PL depolarization in Faraday geometry.

Other possibilities for depolarization can arise from the QW inhomogeneity. Indeed, the studied ultrathin QW is a very inhomogeneous (Ga,Al)(Sb,As) layer, in which the alloy composition strongly fluctuates in the QW plane and along the growth axis. Let us take into account the effects of the exchange interaction between the electron and the hole forming the exciton. The nonzero isotropic exchange interaction splits the exciton state (fourfold degenerate without exchange with total angular momentum projections ± 1 and ± 2) into the doubly degenerate bright and doubly degenerate dark exciton states with ± 1 and ± 2 , respectively. Breaking of the axial symmetry in an inhomogeneous QW mixes the bright exciton states and lifts the degeneracy between them so that the following states emerge: $|X\rangle = \frac{1}{\sqrt{2}}(|+1\rangle + |-1\rangle)$ and $|Y\rangle = \frac{1}{i\sqrt{2}}(|+1\rangle - |-1\rangle)$ [35]. These states are dipole active along two orthogonal principal axes. Therefore, the exciton emission splits into two cross-linearly polarized lines. The

suppression of the circular polarization depends on the energy of the anisotropic exchange interaction (δ_1), by which the states $|X\rangle$ and $|Y\rangle$ are split. In a longitudinal magnetic field, the circular polarization is restored when the exciton Zeeman splitting exceeds the splitting δ_1 between the $|X\rangle$ and $|Y\rangle$ exciton states in a sufficiently high magnetic field [36,37]. Vice versa, in order to suppress the PL circular polarization induced by magnetic field, δ_1 should exceed the exciton Zeeman splitting for all applied magnetic fields. However, we demonstrated recently that in similar structures with indirect band gap the exchange interaction energy is very small [38–40]. That is the result of the small overlap of the wave functions of the X electron and the Γ heavy hole in momentum space [41,42]. Thus, mixing of the exciton states by the anisotropic exchange interaction cannot be considered as a prime reason for the PL depolarization.

One more effect of the composition fluctuations and strain inhomogeneity is the mixing of the heavy and light hole states, which breaks the equivalence of the X and Y orbital Bloch functions in the valence band [43,44]. As a result, the circular polarization is suppressed and linear polarization of emission can appear.

The suppression of circular polarization depends on the mixing strength of light and heavy holes, which, in turn, is determined by the degree of alloy composition inhomogeneity in the QW. The linewidth of the exciton photoluminescence from a thin QW can be used for a rough estimate of the alloy inhomogeneity. We observe a correlation between the PL linewidth in the ultrathin GaAs/AIAs and GaSb/AIAs QWs and the circular polarization degree induced by the longitudinal field. In a magnetic field of 6 T, P_c has values of -0.6 , -0.06 , and less than -0.01 for QWs with PL linewidths of 19 meV (1-ML-thick GaAs/AIAs QW [15]) and 110 meV and 190 meV [the (Ga,Al)(As,Sb)/AIAs QWs studied here], respectively. Thus, the effect of light and heavy hole mixing due to fluctuations of the (Ga,Al)(As,Sb) alloy composition is, likely, the main reason for the PL depolarization. In our recent paper we estimated the depolarizing factor as $\xi = (1 - \eta^2)/(1 + \eta^2)$, where η is the coefficient, describing the mixing of light and heavy holes. $\varphi = \varphi_h + \eta \times \varphi_l$; here φ_h and φ_l are the wave functions of light and heavy holes [16]. For $\xi = 0.25$, we estimate η to be 0.77. Taking into account (i) the strong mixing during the overgrowth of the thin GaSb layer with the AIAs matrix material and (ii) the biaxial strain [45], we estimate that the energy splitting of the heavy hole/light hole lies in the range of 20–30 meV. The strong fluctuations in the composition and well width lead to the possibility that the states of light and heavy holes in spatially adjacent regions can have the same energy, which can lead to a strong mixing of these states.

IV. CONCLUSIONS

The exciton recombination and spin relaxation dynamics in thin indirect band gap (Ga,Al)(Sb,As)/AIAs QWs were studied. It was shown that QWs fabricated on the basis of a GaSb layer with a nominal thickness of less than 1 ML have a type-I band alignment. The exciton lifetime amounts to up to hundreds of microseconds at liquid helium temperature.

The values of the longitudinal heavy-hole g factor (equal to 2.5) as well as of the electron and heavy-hole spin relaxation times (not exceeding 100 ns) were determined. All studied structures demonstrate an unexpectedly low degree of circular polarization in a longitudinal magnetic field. Possible mechanisms responsible for that were discussed among which the change of the heavy-light hole mixing under the influence of strong alloying was identified as the most probable origin. The surprisingly short spin relaxation time, as well as the low degree of the magnetic-field-induced PL circular polarization, reveals that the long lifetime of the localized excitons is not enough to preserve their spin polarization. To clarify the situation with the localized spin conservation, we plan to extend our study to the spin dynamics of long-lived localized excitons in other indirect band gap QWs and QDs formed on the basis

of antimonides, arsenides, and phosphates in the family of A3B5 compounds.

ACKNOWLEDGMENTS

We thank M. M. Glazov for fruitful discussions. This work was supported by the Deutsche Forschungsgemeinschaft via Project No. 409810106 and by the Russian Foundation for Basic Research Grant No. 19-52-12001. T.S.Sh. acknowledges the financial support by the Russian Foundation for Basic Research (Grant No. 19-02-00098) and by Act 211 of the Government of the Russian Federation (Contract No. 02.A03.21.0006). The Government of the Russian Federation also supports this work via Grant No. 0306-2019-0015).

-
- [1] *Spin Physics in Semiconductors*, edited by M. I. Dyakonov (Springer, Berlin, 2008).
- [2] A. Fert, The origin, development and future of spintronics, *Phys. Usp.* **51**, 1336 (2008).
- [3] N. Somaschi, V. Giesz, L. De Santis, J. C. Lored, M. P. Almeida, G. Hornecker, S. L. Portalupi, T. Grange, C. Anton, J. Demory, C. Gomez, I. Sagnes, N. D. Lanzillotti-Kimura, A. Lemaitre, A. Auffeves, A. G. White, L. Lanco, and P. Senellart, Near-optimal single-photon sources in the solid state, *Nat. Photonics* **10**, 340 (2016).
- [4] *Optical Orientation*, edited by F. Meier and B. P. Zakharchenja (North-Holland, Amsterdam, 1984).
- [5] T. S. Shamirzaev, Exciton recombination and spin dynamics in indirect-gap quantum wells and quantum dots, *Phys. Solid State* **60**, 1554 (2018).
- [6] E. L. Ivchenko, Magnetic circular polarization of exciton photoluminescence, *Phys. Solid State* **60**, 1514 (2018).
- [7] D. Dunker, T. S. Shamirzaev, J. Debus, D. R. Yakovlev, K. S. Zhuravlev, and M. Bayer, Spin relaxation of negatively charged excitons in (In, Al)As/AlAs quantum dots with indirect band gap and type-I band alignment, *Appl. Phys. Lett.* **101**, 142108 (2012).
- [8] R. Cingolani and K. Ploog, Frequency and density dependent radiative recombination processes in III-V semiconductor quantum wells and superlattices, *Adv. Phys.* **40**, 535 (1991).
- [9] M. Paillard, X. Marie, P. Renucci, T. Amand, A. Jbeli, and J. M. Gérard, Spin Relaxation Quenching in Semiconductor Quantum Dots, *Phys. Rev. Lett.* **86**, 1634 (2001).
- [10] A. V. Khaetskii and Yu. V. Nazarov, Spin relaxation in semiconductor quantum dots, *Phys. Rev. B* **61**, 12639 (2000).
- [11] A. V. Khaetskii and Yu. V. Nazarov, Spin-flip transitions between Zeeman sublevels in semiconductor quantum dots, *Phys. Rev. B* **64**, 125316 (2001).
- [12] M. Kroutvar, Y. Ducommun, D. Heiss, M. Bichler, D. Schuh, G. Abstreiter, and J. J. Finley, Optically programmable electron spin memory using semiconductor quantum dots, *Nature (London)* **432**, 81 (2004).
- [13] T. S. Shamirzaev, Type I semiconductor heterostructures with an indirect gap conduction band, *Semiconductors* **45**, 96 (2011).
- [14] D. S. Abramkin and T. S. Shamirzaev, Type-I indirect-gap semiconductor heterostructures on (110) substrates, *Semiconductors* **53**, 703 (2019).
- [15] T. S. Shamirzaev, J. Debus, D. R. Yakovlev, M. M. Glazov, E. L. Ivchenko, and M. Bayer, Dynamics of exciton recombination in strong magnetic fields in ultrathin GaAs/AlAs quantum wells with indirect band gap and type-II band alignment, *Phys. Rev. B* **94**, 045411 (2016).
- [16] T. S. Shamirzaev, J. Rautert, D. R. Yakovlev, J. Debus, A. Yu. Gornov, M. M. Glazov, E. L. Ivchenko, and M. Bayer, Spin dynamics and magnetic field induced polarization of excitons in ultrathin GaAs/AlAs quantum wells with indirect band gap and type-II band alignment, *Phys. Rev. B* **96**, 035302 (2017).
- [17] T. S. Shamirzaev, J. Rautert, D. R. Yakovlev, M. M. Glazov, and M. Bayer, Intrinsic and magnetic-field-induced linear polarization of excitons in ultrathin indirect-gap type-II GaAs/AlAs quantum wells, *Phys. Rev. B* **99**, 155301 (2019).
- [18] T. S. Shamirzaev, D. S. Abramkin, A. K. Gutakovskii, and M. A. Putyato, High quality relaxed GaAs quantum dots in GaP matrix, *Appl. Phys. Lett.* **97**, 023108 (2010).
- [19] D. S. Abramkin, K. M. Rumynin, A. K. Bakarov, D. A. Kolotovkina, A. K. Gutakovskii, and T. S. Shamirzaev, Quantum dots formed in InSb/AlAs and AlSb/AlAs heterostructures, *JETP Lett.* **103**, 692 (2016).
- [20] T. S. Shamirzaev, D. S. Abramkin, A. K. Gutakovskii, and M. A. Putyato, Novel self-assembled quantum dots in the GaSb/AlAs heterosystem, *JETP Lett.* **95**, 534 (2012).
- [21] The structure S2 was used as an example of thin GaSb/AlAs QWs in our recent study [24].
- [22] T. S. Shamirzaev, J. Debus, D. S. Abramkin, D. Dunker, D. R. Yakovlev, D. V. Dmitriev, A. K. Gutakovskii, L. S. Braginsky, K. S. Zhuravlev, and M. Bayer, Exciton recombination dynamics in an ensemble of (In, Al)As/AlAs quantum dots with indirect band-gap and type-I band alignment, *Phys. Rev. B* **84**, 155318 (2011).
- [23] D. Keller, D. R. Yakovlev, B. König, W. Ossau, Th. Gruber, A. Waag, L. W. Molenkamp, and A. V. Scherbakov, Heating of the magnetic ion system in (Zn, Mn)Se/(Zn, Be)Se semimagnetic quantum wells by means of photoexcitation, *Phys. Rev. B* **65**, 035313 (2001).
- [24] D. S. Abramkin, A. K. Gutakovskii, and T. S. Shamirzaev, Heterostructures with diffused interfaces: Luminescent technique for ascertainment of band alignment type, *J. Appl. Phys.* **123**, 115701 (2018).

- [25] C. W. Snyder, B. G. Orr, D. Kesler, and L. M. Sander, Kinetically Controlled Critical Thickness for Coherent Islanding and Thick Highly Strained Pseudomorphic Films of $\text{In}_x\text{Ga}_{1-x}\text{As}$ on GaAs(100), *Phys. Rev. Lett.* **66**, 3032 (1991).
- [26] D. E. Jesson, S. J. Pennycook, J.-M. Baribeau, and D. C. Houghton, Direct Imaging of Surface Cusp Evolution During Strained-Layer Epitaxy and Implications for Strain Relaxation, *Phys. Rev. Lett.* **71**, 1744 (1993).
- [27] P. Muller and R. Kern, The physical origin of the two-dimensional towards three-dimensional coherent epitaxial Stranski-Krastanov transition, *Appl. Surf. Sci.* **102**, 6 (1996).
- [28] I. Vurgaftman, J. R. Meyer, and L. R. Ram-Mohan, Band parameters for III-V compound semiconductors and their alloys, *J. Appl. Phys.* **89**, 5815 (2001).
- [29] D. S. Abramkin, M. A. Putyato, S. A. Budenny, A. K. Gutakovskii, B. R. Semyagin, V. V. Preobrazhenskii, O. F. Kolomys, V. V. Strelchuk, and T. S. Shamirzaev, Atomic structure and energy spectrum of Ga(As, P)/GaP heterostructures, *J. Appl. Phys.* **112**, 083713 (2012).
- [30] D. S. Abramkin, V. T. Shamirzaev, M. A. Putyato, A. K. Gutakovskii, and T. S. Shamirzaev, Coexistence of type-I and type-II band alignment in Ga(Sb, P)/GaP heterostructures with pseudomorphic self-assembled quantum dots, *JETP Lett.* **99**, 76 (2014).
- [31] D. S. Abramkin, A. K. Bakarov, A. K. Gutakovskii, and T. S. Shamirzaev, Spinodal decomposition in InSb/AlAs heterostructures, *Semiconductors* **52**, 1392 (2018).
- [32] J. Debus, T. S. Shamirzaev, D. Dunker, V. F. Sapega, E. L. Ivchenko, D. R. Yakovlev, A. I. Toropov, and M. Bayer, Spin-flip Raman scattering of the Γ -X mixed exciton in indirect band gap (In, Al)As/AlAs quantum dots, *Phys. Rev. B* **90**, 125431 (2014).
- [33] V. Yu. Ivanov, T. S. Shamirzaev, D. R. Yakovlev, A. K. Gutakovskii, Ł. Owczarczyk, and M. Bayer, Optically detected magnetic resonance of photoexcited electrons in (In, Al)As/AlAs quantum dots with indirect band gap and type-I band alignment, *Phys. Rev. B* **97**, 245306 (2018).
- [34] P. S. Alekseev, M. V. Yakunin, and I. N. Yassievich, Influence of the spin-orbit interaction on the spectrum of 2-D electrons in the magnetic field, *Semiconductors* **41**, 1092 (2007).
- [35] M. Bayer, G. Ortner, O. Stern, A. Kuther, A. A. Gorbunov, A. Forchel, P. Hawrylak, S. Fafard, K. Hinzer, T. L. Reinecke, S. N. Walck, J. P. Reithmaier, F. Klopff, and F. Schäfer, Fine structure of neutral and charged excitons in self-assembled In(Ga)As/(Al)GaAs quantum dots, *Phys. Rev. B* **65**, 195315 (2002).
- [36] R. I. Dzhioev, H. M. Gibbs, E. L. Ivchenko, G. Khitrova, V. L. Korenev, M. N. Tkachuk, and B. P. Zakharchenya, Determination of interface preference by observation of linear-to-circular polarization conversion under optical orientation of excitons in type-II GaAs/AlAs superlattices, *Phys. Rev. B* **56**, 13405 (1997).
- [37] M. Sénès, B. Urbaszek, X. Marie, T. Amand, J. Tribollet, F. Bernardot, C. Testelin, M. Chamarro, and J. M. Gérard, Exciton spin manipulation in InAs/GaAs quantum dots: Exchange interaction and magnetic field effects, *Phys. Rev. B* **71**, 115334 (2005).
- [38] J. Rautert, M. V. Rakhlin, K. G. Belyaev, T. S. Shamirzaev, A. K. Bakarov, A. A. Toropov, I. S. Mukhin, D. R. Yakovlev, and M. Bayer, Anisotropic exchange splitting of excitons affected by ΓX mixing in (In, Al)As/AlAs quantum dots: Microphotoluminescence and macrophotoluminescence measurements, *Phys. Rev. B* **100**, 205303 (2019).
- [39] M. S. Kuznetsova, J. Rautert, K. V. Kavokin, D. S. Smirnov, D. R. Yakovlev, A. K. Bakarov, A. K. Gutakovskii, T. S. Shamirzaev, and M. Bayer, Electron-nuclei interaction in X valley of (In, Al)As/AlAs quantum dots, *Phys. Rev. B* **101**, 075412 (2020).
- [40] J. Rautert, T. S. Shamirzaev, S. V. Nekrasov, D. R. Yakovlev, P. Klenovský, Yu. G. Kusrayev, and M. Bayer, Optical orientation and alignment of excitons in direct and indirect band gap (In, Al)As/AlAs quantum dots with type-I alignment, *Phys. Rev. B* **99**, 195411 (2019).
- [41] G. L. Bir and G. E. Pikus, *Symmetry and Strain-Induced Effects in Semiconductors* (Wiley, New York, 1974).
- [42] G. E. Pikus and G. L. Bir, Exchange interaction in excitons in semiconductors, *Zh. Eksp. Teor. Fiz.* **60**, 195 (1971) [*Sov. Phys. JETP* **33**, 108 (1971)].
- [43] G. E. Pikus and F. G. Pikus, The mechanism of heavy and light hole mixing in GaAs/AlAs superlattices, *Solid State Commun.* **89**, 319 (1994).
- [44] E. L. Ivchenko, A. Yu. Kaminski, and U. Roessler, Heavy-light hole mixing at zinc-blende (001) interfaces under normal incidence, *Phys. Rev. B* **54**, 5852 (1996).
- [45] T. S. Shamirzaev, A. M. Gilinsky, A. K. Kalagin, A. V. Nenashev, and K. S. Zhuravlev, Energy spectrum and structure of thin pseudomorphic InAs quantum wells in an AlAs matrix: Photoluminescence spectra and band-structure calculations, *Phys. Rev. B* **76**, 155309 (2007).